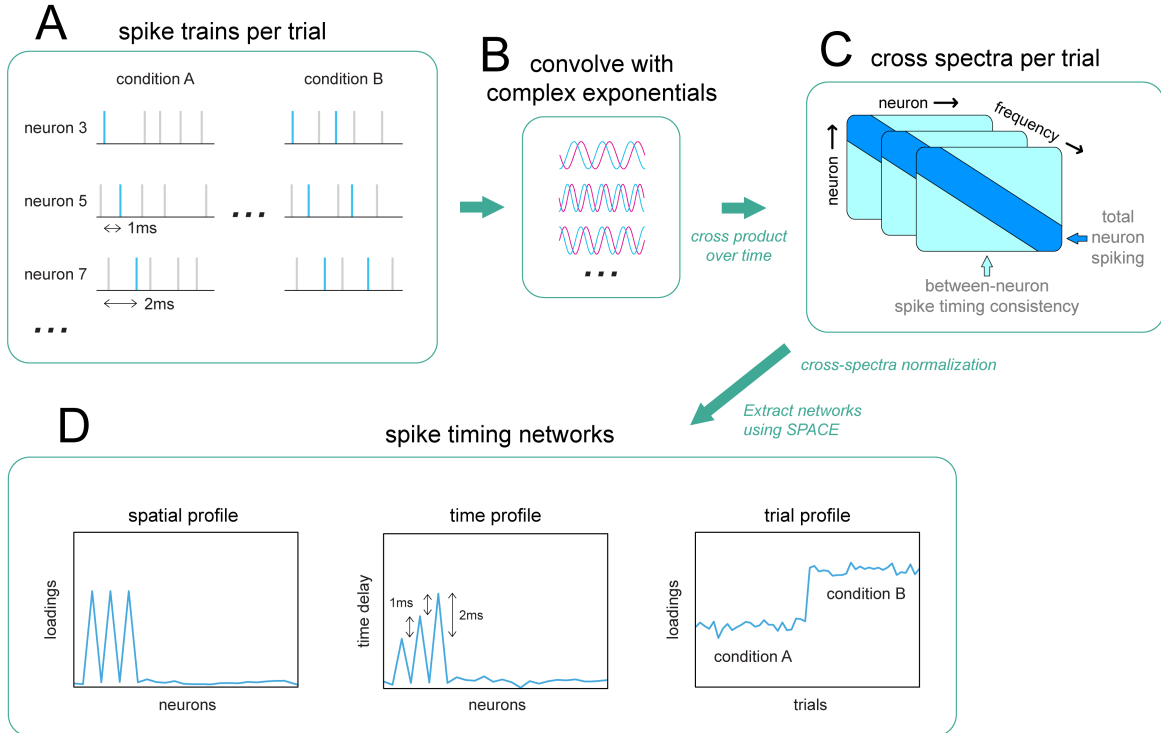


## Materials and Methods

### 1. Extracting spiking timing networks from neural spike recordings

Spike timing consistency between neurons is thought to indicate a functional relationship. Here, we present how a recent technique (SPACE; van der Meij et al., 2015, 2016) can be used to find consistent spike timing of multiple neurons, forming so-called spike timing networks, in large scale neural spike recordings. These spike timing networks can be of arbitrary size, and have arbitrary time delays between spikes in their spike sequence, and can be found without a priori information on which neurons are involved, or at which timing. Once found, the spike timing networks provide a description of the structure of spike timing consistency in the recording, and can be used to conduct a targeted investigation into their spike sequences: e.g., does the reliability of the individual spike times relate to experimental variables, do spike sequences occur more often in certain conditions, or does the completeness of the spike sequence change in the course of the experiment.

The procedure to extract spike timing networks is illustrated in Figure 1, it is briefly described here, and in more detail in dedicated sections. We start with multi-electrode neural recordings over time  $t$  of which neurons  $J$  and their spikes have been identified (using e.g. Rossant et al., 2016), and arrange the detected spikes in neuron-by-time ( $J \times t$ ) binary matrices  $S_l$  (Fig 1A; 1 = spike, 0 = no spike), per trial  $l$  of the experiment (or any other meaningful temporal segmentation). Then, we obtain ‘cross spectra’ from these trial-specific matrices. To achieve this, we first convolve the matrices  $S_l$  with complex exponentials at multiple frequencies  $k$ , resulting in frequency-specific and trial-specific complex-valued neuron-by-time ( $J \times t$ ) matrices  $Z_{kl}$ . Subsequently, we compute the cross products  $Z_{kl}Z_{kl}^*$  of these matrices over time (\* = complex conjugate transpose), resulting in complex-valued frequency-specific and trial-specific neuron-by-neuron ( $J \times J$ ) matrices  $X_{kl}$ : the cross spectra (Fig 1B). The choice of complex exponentials determines key aspects of the spike timing networks and their extraction, and is discussed in detail in Materials and Methods section 3. From the cross spectra, we can extract spike timing networks. Prior to extraction we can apply a neuron-wise and/or trial-wise normalization if desired (see Materials and Methods section 4). The extraction technique, denoted as SPACE, describes the systematic variability of the cross spectra by multiple networks, each network consisting of three parameter vectors (Fig 1C): the *spatial profile* ( $1 \times J$ ), the *time profile* ( $1 \times J$ ), and the *trial profile* ( $1 \times L$ ). The spatial profile describes how strongly each neuron is part of the network, by a single number per neuron. The time profile describes the temporal sequence of the network, by a single number per neuron indicating its time delay with respect to the other neurons. When used jointly with the spatial profile to select neurons, the time profile reflects the spike sequence of the network. Lastly, the trial profile describes how strongly the network is present in each trial, by a single number per trial. This can, in principle, be used an index of network activity, allowing for comparing neural activity between conditions at the level of networks instead of at the level of individual neurons. Networks can be extracted from the cross spectra, because the phases of the off-diagonal elements of the cross spectra describe the consistent time delays between spikes. The crucial principle here, is that time differences in the time domain translate to phase differences in the frequency domain, and that these phase differences increase linearly with frequency. That is, a 1ms time delay equals  $1/20^{\text{th}}$  of a cycle at 50Hz,  $1/10^{\text{th}}$  at 100Hz,  $1/5^{\text{th}}$  at 200Hz, etc. The technique used here uses this property to find the time delays between neurons that explains the most variance in the cross spectra.



**Figure 1. Extracting spike timing networks.** To extract spike timing networks, we start with binary spike trains of multiple neurons, arranged in a neuron-by-time matrix. These spike trains are then convolved with complex exponentials (or ‘wavelets’) of equal length, but varying frequency, resulting in a complex-valued neuron-by-time matrix per frequency per trial. The cross products are then computed along the time dimension, resulting in a neuron-by-neuron cross-product matrix per frequency per trial: the cross spectrum. Using the between-neuron phases of the cross spectra over frequencies, spike timing networks can be extracted. Each network is described by a spatial profile, having a single weight per neuron, a time profile, describing the spike sequence by a time coefficient per neuron, and a trial profile, having a single weight per trial. For details see Materials and Methods section 1,2, and 3.

## 2. SPACE describes time consistency induced phase coupling in cross spectra

SPACE is a decomposition technique that describes the structure of phase coupling in cross spectra by time delays between neurons (or electrodes/sensors/sites). The algorithm is extensively treated in its original publication ((van der Meij et al., 2015), but see also (van der Meij et al., 2016) for an alternate presentation), and only elements essential to its current use will be mentioned here. The usage of the technique in the current paper is identical to that in the original publication (referred to as SPACE-time therein). The only difference lies in how the input, i.e. the cross spectra, are computed. Briefly, the technique consists of an Alternating Least Squares (ALS) algorithm to find the least squares estimates of its decomposition model. The element-wise formulation of this model for the cross spectra is likely the most insightful:

$$X_{j_1 j_2 k l} = \sum_{f=1}^F (a_{j_1 f} \cdot a_{j_2 f}) \cdot \exp(i 2\pi \varphi_k (\sigma_{j_1 f} - \sigma_{j_2 f})) \cdot b_{k f}^2 \cdot c_{l f}^2 + \varepsilon_{j_1 j_2 k l}$$

The complex-valued cross spectrum ( $X_{j_1 j_2 k l}$ ) of neurons  $j_1$  and  $j_2$  at frequency  $k$  and trial  $l$  is described as the product of network parameters, summed over networks  $F$ , plus an error term  $\varepsilon_{j_1 j_2 k l}$ . The phase of the network-specific product is given by the difference in the time profile ( $\sigma_{j_1 f} - \sigma_{j_2 f}$ ) of neuron  $j_1$  and  $j_2$  multiplied by the frequency  $\varphi_k$  in Hz, multiplied by  $2\pi$ . This phase is then weighted by the product of the two neurons’ spatial profile  $a_{j_1 f} \cdot a_{j_2 f}$ , the (squared) frequency profile  $b^2$  at frequency  $k$ , and the (squared) trial profile  $c^2$  at trial  $l$ . As is observed here, the technique also produces a *frequency profile* per network, describing how important each frequency is for a network. For the purpose of spike timing

networks, we will ignore this, as it does not provide additional information. It is, however, an essential element of its original application on electrophysiological recordings, describing frequency band-specific phase-coupled oscillatory networks, such as traveling waves. The careful reader comparing the above to the reference publications, will notice the present explicit squaring of the trial and frequency profile. Note that the model remains identical to that in the reference publications. The reason for the explicit squaring, is that spike timing networks are more conveniently thought of, analyzed at, and simulated in, the description level of cross spectra. This is not the case for phase-coupled oscillatory networks, which are more conveniently thought of as time-varying oscillations over electrodes described by Fourier coefficients (of which the cross products over time produce the cross spectra). Due to this, the technique provides trial and frequency profiles that are not squared, and squaring becomes a necessary step prior to analyzing spike timing networks that were extracted.

The three profiles of each spike timing network have trivial indeterminacies, that are easily resolved by normalizations. These indeterminacies are a consequence of the technique and its underlying model, and are discussed in detail in the original publication (van der Meij et al., 2015). Here, we briefly highlight the normalizations and their consequences as they pertain to spike timing networks. The spatial and trial profiles, per network, have undetermined multiplicative scaling, and are normalized to have a vector L2-norm of 1. The consequence is that the absolute values of neurons and trials only have meaning w.r.t. the other neurons and trials of the same network. Crucially, the ratios between neurons and trials are unaffected by this normalization, and can be compared freely across networks. Additionally, their sign is also undetermined, and restricted to have a positive average per network (spatial profile) or to be fully positive (trial profile). The indeterminacy of the time profile is more complicated. Because the time profile describes circular phases over multiple frequencies, the time profile is circular as well. In short, we normalize it such that the strongest neuron (of the spatial profile) has a time profile of 0. Due to the circularity, time differences between neurons can be interpreted as long as the biggest difference between neurons is equal to half of the time-window length of the complex exponentials (when computing cross spectra as described in the section below). Finally, due to the above normalizations, a network-specific multiplicative scaling parameter is also extracted, but it does not play a role in the interpretation of the individual network parameters.

Two practical points need to be made for using the technique to extract networks. The first is that its algorithm is initialized from random starting values. In order to avoid unfortunate starting values that lead to a local minimum of its least squares loss function, the algorithm needs to be initialized multiple times. When it converges to the same solution multiple times, it can be assumed the global minimum (i.e. the desired decomposition) is reached. The second practical point is that, like related decomposition techniques, the number of networks to extract should be estimated. One approach is to estimate the number of *reliable* networks. For this, we split a recording in two halves, the first containing the odd numbered spikes of each neuron, the second the even numbered spikes. N networks are then extracted from the full recording and the two splits. If the networks from both splits match those of the full recording, N is increased, and the process is repeated until they no longer match. To determine whether two networks match, a coefficient can be computed for the three parameters of the networks. For the spatial and the trial profiles, this is simply the inner product between the L2-normalized profiles of two networks, and ranges from 0 to 1 (identical profiles). For the time profile, a coefficient is the following:

$$\text{time profile similarity: } |\langle A^1 \cdot \exp(i2\pi\gamma\sigma^1), A^2 \cdot \overline{\exp(i2\pi\gamma\sigma^2)} \rangle|$$

Time profile similarity is computed as the absolute value  $|\cdot|$  of the inner-product  $\langle \cdot, \cdot \rangle$  over neurons  $J$  of the time profiles  $\sigma$  of two networks (superscript 1 and 2,  $\bar{\cdot}$  denotes complex conjugate), weighted by the normalized spatial profiles  $A$  of each network ( $\cdot$  denotes the element-wise product). Here,  $\gamma$  stands for the greatest common divisor of the frequencies used to extract the network (50Hz in this case), in

Hz, which determines the ‘cycle length’ of the circular time profile (van der Meij et al., 2015). This similarity coefficient also ranges from 0 to 1 (identical profiles).

The technique is publically available in a GitHub repository termed *nwaydecomp* ([www.github.com/roemervandermeij/nwaydecomp](https://www.github.com/roemervandermeij/nwaydecomp)), together with tutorials on its use. The toolbox also contains software to deal with the practical points above.

### 3. Obtaining cross spectra that are optimal for extracting spike timing networks

To be able to extract spike timing networks we compute cross spectra from binary spike trains, by convolving the spike trains with complex exponentials (‘wavelets’) and computing their cross products over time. Doing so transforms the time delays between spikes of different neurons, into phase differences at multiple frequencies. The choice of complex exponentials determines how sensitive the cross spectra are to consistent vs non-consistent time delays, and is described in the following. Here, it is important to realize that the cross spectrum between two neurons, is *exactly* the complex-valued sum of the time delay induced phase differences between any pair of their spikes who temporally overlap after the convolution, weighted by the amount of overlap. Due to the latter, long time delays necessarily have lower weighting than short time delays.

The time domain length of the complex exponentials determines which between-spike time delays can contribute to the cross spectra, and it should be chosen based on the expected range of time delays. Presently, we wish to be sensitive to time delays between 0 and 10ms. The optimal time domain length for an expected range is a trade-off. The longer the length, the lower the sensitivity will be to the expected time delays, as the cross spectra will contain more spike pairs at ‘uninteresting’ time delays. The shorter the length, the bigger the difference in weighting between the shortest and the longest expected time delay, and thus the stronger the bias towards the former. As a compromise, we choose a length of 20ms. In order to further reduce the bias of short time delays to long time delays, the complex exponentials should have constant magnitude, and not be tapered using a particular windowing function.

The frequencies of the complex exponentials greatly determine the sensitivity of the cross spectra to non-consistent time delays. In order to be maximally sensitive to consistent time delays, the contribution to the cross spectrum of all other time delays should be as small as possible. In the terms of phase differences in the cross spectra, this is achieved when the average of the complex-valued phase differences of the non-consistent time delays approaches a magnitude of 0. This is the case for any frequency whose cycle length is an integer multiple of the time domain length chosen above (for 20ms, 50Hz, 100Hz, 150Hz, etc), under the assumption that non-consistent spike pairs are equally likely at any time delay. To arrive here, it is crucial to appreciate the fact that phase differences for large time delays are weighted lower than those for small time delays. For phase differences originating from time delays between 0ms and the time domain length (20ms above) to have an average magnitude of 0, the weighting coefficients for phase differences between  $\pi/2$  to  $-\pi/2$ , the left side/quadrant 2 and 3 of the unit circle, need to have the same sum as those for  $-\pi/2$  to  $\pi/2$ , the right side/quadrant 1 and 4 of the unit circle. Crucially, for the frequency whose cycle length equals the maximum time delay, the 25% smallest time delays fall in quadrant 1, the middle 50% of time delays fall in quadrant 2 and 3, and the 25% largest time delays fall in quadrant 4. Equally crucial, the weighting is a linear function of the time delays. As for any linear function the sum of the first 25% and the last 25% of a subset of its values is equal to the sum of its middle 50%, the frequency with a cycle length equaling the largest time delay will have phase differences from non-consistent time delays that approach an average magnitude of 0. This also holds for any integer multiple N of this frequency, as the above will be the case for N equal splits of the time delay range. Note that to obtain an average magnitude of 0, it is also required that the sum of weighting coefficients for quadrant 1 and 2 (top of unit circle) is equal to that of quadrant 3 and 4 (bottom of unit circle). This symmetry is easily achieved however, as the weighting coefficients for -

20ms to 0ms progress along the unit circle in opposite direction than those for +20ms to 0ms. As a last note, the frequencies of the complex exponentials also determine the robustness to jitter around a consistent time delay. The lower the frequency, the closer the phases of jittered but consistent time delays, the higher their average magnitude, and thus, the more robust to jitter.

Concluding, we compute cross spectra by convolving spike trains with complex exponentials of 20ms length, constant magnitude, and at 20 frequencies from 50Hz to 1000Hz in steps of 50Hz. When investigating longer time-scale neural dynamics, an analogous set would be e.g. 1s length, at 1Hz to 20Hz in steps of 1Hz. The number of frequencies to use is somewhat arbitrary. Initial simulations showed no noticeable difference beyond 20 frequencies (and 1000Hz is already very sensitive to jitter), and in the original publication of the technique, networks were reliably recovered from simulations with as little as 5 involved frequencies.

#### 4. Normalizations of the cross spectra

The spatial profiles of spike timing networks describe the off-diagonal elements of each cross spectrum, reflecting between-neuron spike pairs, and the diagonal elements, i.e. power, reflecting the total number of spikes of neurons. In realistic data, the firing rates of neurons can differ greatly, resulting in large differences in power. Because the power of each cross spectrum is typically much larger than its off-diagonal elements, this can lead to spike timing networks whose spatial profiles are driven more by power differences between neurons, than differences in the magnitude of the off-diagonal elements. To increase sensitivity to the latter, power differences between neurons can be normalized to decrease their impact. Normalizing power such that it is equal to an Nth root is one such normalization:

$$\text{neuron-wise normalization: } X_{j_1 j_2 k l} = X_{j_1 j_2 k l} \frac{\sum_K \sum_L |X_{j_1 j_2 k l}|^{1/N}}{\sum_K \sum_L |X_{j_1 j_2 k l}|}$$

Here,  $| \cdot |$  indicates the absolute value. By increasing N, the power differences between neurons decrease. This could be taken to the extreme, by normalizing the cross spectra such that neurons have equal power: i.e. coherency spectra. This however, has the unintended consequence of making networks of similar size have similar amounts of explained variance (strengthened by the noise sensitivity of the trial profile, see e.g. Results section 2). Because the least squares algorithm is randomly initialized, reduced differences in explained variance between networks increases the variability in the order with which networks are extracted, as small variations in the random starting values become more influential. When using a split-half reliability estimation of the number of networks to extract, this is problematic, as splits become unlikely to contain the same networks. As such, it is advisable to choose an Nth root power normalization that still extracts a useful number of networks.

The firing rate of neurons can also differ greatly between trials. As the trial profile reflects the weight of a spike timing network in each trial, they reflect both the firing rate of the involved neurons as well as their spike timing consistency. Similar to the above, normalizing the cross spectra over trials can reduce the impact of firing rate on the trial profile. Normalizing power such that it is equal across trials is one such normalization:

$$\text{trial-wise normalization: } X_{j_1 j_2 k l} = X_{j_1 j_2 k l} \frac{\sum_L |X_{j_1 j_2 k l}|}{|X_{j_1 j_2 k l}|}$$

This normalization is independent of the above neuron-wise normalization, both normalizations can be applied jointly. Note that the above normalization removes a lot of variability in the cross spectra, potentially distorting structure in the cross spectra necessary for identifying networks. As such, it can be advisable to first extract networks from non-trial-normalized cross spectra, and subsequently re-estimate their trial profiles by using the extracted network parameters as starting values for extracting networks from the trial-normalized cross spectra, holding their spatial and time profiles constant.

## 5. Simulating and extracting noisy spike timing networks

To investigate the effects of various kinds of noise on spike timing network extraction, we simulated spike recordings of 15 neurons at 100 trials of 1s containing 4 spike timing networks. Network spiking sequences had a fixed temporal structure that was repeated between 0 or 3 (predetermined) times per trial (1.2Hz average spiking rate over all trials for each network). Within each trial, each spike sequence could occur anywhere with uniform probability, with a 25ms offset from trial boundaries. On trials where spike sequences of multiple networks were present their order was randomized, and with a minimum of 25ms between sequences. Three kinds of noise were simulated. First, all neurons of a single simulation had a noise spiking rate of 0Hz, 5Hz, 10Hz, 20Hz, or 100Hz, as Poisson spiking superimposed on the network spike sequences. Second, each spike of each spike sequence could have an individual random jitter (uniformly distributed) at a maximum of 0ms,  $\pm 0.25\text{ms}$ ,  $\pm 0.5\text{ms}$ ,  $\pm 1\text{ms}$ , or  $\pm 2\text{ms}$ . Third, each spike of each spike sequences had an individual deletion probability of 0%, 10%, 20%, 40%, 80%, resulting in sparseness of the spike sequences. Cross spectra of each simulation run were obtained as described above, using a time-window length of 20ms and frequencies from 50Hz to 1000Hz in steps of 50Hz. The 4 networks were extracted using 10 random initializations of the extraction algorithm. Note that the purpose of these simulations is to show how well a particular spiking pattern can be extracted under noisy conditions, and not how such a pattern can be generated physiologically, nor whether such a pattern is physiologically meaningful.

## 6. Quantifying recovery of simulated spike timing networks

To quantify the recovery of the extracted spatial profile, time profile, and the trial profile, they were compared to the simulated equivalents. The simulated spatial profiles were constructed as a binary  $1 \times J$  vector per network, its values indicating network membership of each neuron. Similarly, simulated trial profiles were constructed as  $1 \times L$  vector, its values reflecting the number of sequence repeats. Finally, simulated time profiles were constructed as a  $1 \times J$  vector, its values describing the temporal sequence of spikes in seconds (non-member neurons set arbitrarily to 0). For display purposes these simulated parameters were normalized in the same manner as the extracted network parameters. In order to compute recovery, extracted networks were paired to the simulated networks using the similarity coefficients described above, by first determining the most similar pair, then the next most similar in the remainder, etc. Recovery of spatial and trial profiles was determined using a Pearson correlation coefficient. Time profile recovery was judged by the following coefficient:

$$\text{time profile recovery: } \frac{|\sum_j \exp(i2\pi\gamma\sigma^e) \cdot \overline{\exp(i2\pi\gamma\sigma^s)} \cdot A^s|}{\sum_j A^s}$$

Time profile recovery is computed as the absolute value  $|\cdot|$  of the weighted sum over neurons  $J$  of the complex-valued difference of the circular time profiles  $\sigma$  of the extracted and simulated networks (superscript  $e$  and  $s$  resp.;  $\overline{\cdot}$  denotes complex conjugate), weighted by the simulated spatial profile  $A$  ( $\cdot$  denotes the element-wise product). Similar to the similarity coefficient described above,  $\gamma$  is the greatest common divisor of the frequencies used for extraction (here, 50Hz), and is used to deal with the circularity of the time profile. This coefficient also ranges from 0 to 1 (perfect recovery).

## 7. Extracting spike timing networks from recordings of rat medial prefrontal cortex and hippocampus

As a proof of principle, we extracted spike timing networks from real spiking recordings, obtained from a publically available dataset (Fujisawa et al., 2008, 2014). This dataset contains identified neurons and their spikes from recordings obtained from rat medial prefrontal cortex and area CA1 of the hippocampus, while the rat performed an odor-based delayed matching-to-sample task, requiring it to run through either the left or right arm of a maze to obtain its reward. The recording used (rat GG.069) was sampled at 20kHz and contained 20 left and 20 right trials, having an average duration of 8.04s (SD = 1.73s). Only neurons with average spiking rates of 1Hz and above were selected. In order to extract

networks, we first obtained cross spectra as described in Materials and Methods section 3, using a time window of 20ms and frequencies from 50Hz to 1000Hz in steps of 50Hz, dividing each cross spectra by its trials' duration. Subsequently, cross spectra were neuron-wise normalized as described above, such that their power was equal to its 32<sup>nd</sup> root. The number of networks to extract was determined using odd-even spike split reliability procedure described in Materials and Methods section 2 with a similarity coefficient cut-off of 0.7, 50 random initializations were used at each step. This result in 4 networks being extracted. Continuous cross-correlograms were obtained for spike-pairs that fell within  $\pm 20\text{ms}$  of each, and were computed by addition of their neurons' binary spike trains convolved by a Gaussian with a full-width half-maximum of 0.5ms normalized to a maximum of 1.

## Results

Spike timing networks are formed when multiple neurons have consistent temporal delays between their spikes, i.e. form a spike sequence. Such networks can overlap spatially, with neurons partaking in multiple networks, and temporally, with spike sequences of multiple networks being present in the same time window. Here, we show how a recent method can be used to extract and separate these networks from neural recordings (van der Meij et al., 2015). First, we evaluate its robustness to various noise conditions. We show how the recovery of simulated spike timing networks is affected by spike jitter in the network spike sequences and sparseness of neuron participation in the network, under increasing spiking noise of all simulated neurons. Then, we show how variable firing rates of neurons affects recovery, and what actions can be taken to reduce negative effects. Finally, we provide a proof-of-principle by showing networks extracted from rat hippocampus and medial prefrontal cortex (Fujisawa et al., 2008, 2014), and compare the extracted spike timing relations to pair-wise statistics between the involved neurons.

### 1. Simulated spike recordings from spike timing networks

To investigate the robustness of spike-timing network extraction to various kinds of noise we simulated spike recordings of 15 neurons over 100 trials of 1s containing 4 networks (see Materials and Methods section 5). The networks had overlap in their neurons, and on which trials their spike sequences were present. Spike sequences had time delays between 0 (synchronous) and 2.5ms between its spikes. The simulated networks are shown in Figure 2 in the same representation as extracted networks. That is, each network consists of (1) a *spatial profile*, describing which neurons contribute to the network (Fig 2A first row), (2) a *time profile*, describing the network spiking sequences (Fig 2A second row; only network member neurons are shown), and, (3), a *trial profile*, describing how strongly the network is present on each trial (Fig 2A third/fourth row). Importantly, the absolute values of the spatial and trial profiles are not meaningful, only the *within-network ratios* are (see Materials and Methods section 2). As such, it is not the spike sequence repeats per trial that is described by the trial profile (i.e. 0, 1, 2, 3; Fig 2A second/third row), but rather the ratio between them (e.g. a trial with 3 sequences having a weight 3x that of a 1 sequence trial). The simulated networks were different in size, spike sequence timing, spatial overlap, and temporal overlap, to increase the likelihood that any related weaknesses of the used technique would be revealed. Three kinds of noise were simulated: (1) spiking noise, or non-network spikes, superimposed on the spike sequences (see Fig 2B), (2) jitter of each spike in a spike sequence occurrence, and, (3) sparseness of network spike sequences.

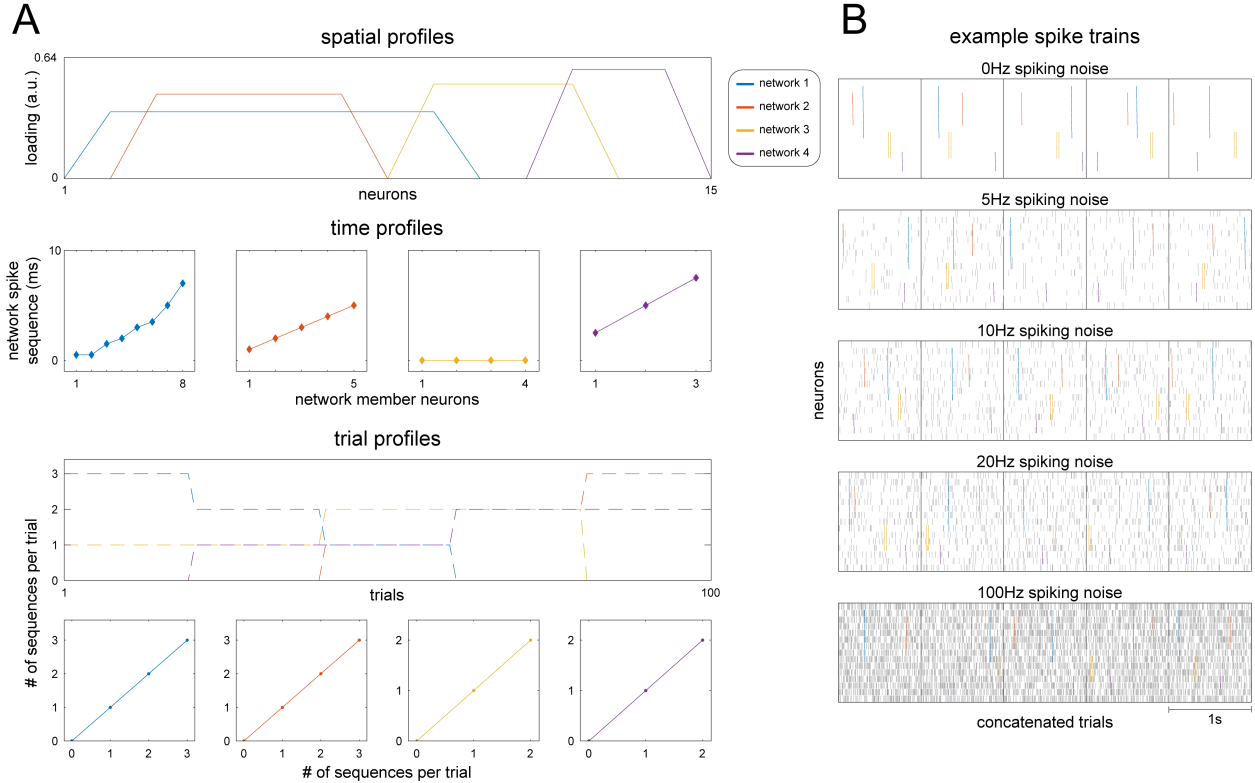


**Figure 2. Simulated spike timing networks.** To investigate the robustness of network extraction to various kinds of noise we simulated spike recordings from 15 neurons containing 4 spike timing networks across 100 trials. **A**, description of simulated networks in same format as extracted networks. The spatial profile of each network describes non-member neurons by 0s and member neurons by 1s. Because absolute magnitudes of the spatial and trial profiles of networks are not meaningful, they are L2-normalized by convention (leading to arbitrary between-network amplitude differences); the between-neuron/trial ratios are meaningful. The second panel shows the temporal spiking sequence of each network, as their time profiles. Each network spiking sequence was present 0-3 times in each trial, described by the trial profiles in the third panel. For convenient display they are not L2-normalized here. The extracted trial profiles are normalized, and perfect recovery is defined as the correspondence of the ratios between trial weights to the ratios of the number of spike sequences. The fourth (set of) panel(s) displays a trial profile summary, as the mean (STD) of the number of sequences/weights for each category of sequence repeats. As this is a convenient way to show recovery, it is used in favor of the first throughout the Results. **B**, raster plots of example spike trains as a function of spiking noise levels used in the simulations. Each vertical dash is a single spike. Each row consists of 5 concatenated trials, separated by a vertical line. Network spiking sequences are shown by their color as in A. See Materials and Methods section 5.

## 2. Recovery of simulated spike timing networks with spiking jitter when surrounded by spiking noise

Neurons are active in many circumstances and not selectively during a single stimulus. As such, any spike sequence of a spike timing network is likely embedded in other spikes of the same neurons.

Furthermore, precise spike times depend on the fluctuating membrane potential of the neuron and other factors, potentially adding temporal jitter. To investigate how these two factors influence network characterization, we simulated spike timing networks with different levels of background spiking noise and with different levels of jitter of each spike in the spike sequences. Networks were simulated 50 times for each combination of the noise factors. We computed recovery of simulated networks and show the result in Figure 3. Recovery of the spatial and trial profiles was computed as the Pearson correlation between the recovered and simulated profiles. Recovery of the time profiles was computed using a recovery coefficient that ranges from 0 to 1 (perfect recovery; see Materials and Methods section 2).

Firstly, we observe that with reasonable jitter (e.g.  $\pm 0.25\text{ms}$  vs  $0\text{-}2.5\text{ms}$  spike sequence delays) and spiking noise (e.g.  $20\text{Hz}$  vs  $1.2\text{Hz}$  average network spiking rate) the spatial and time profiles are

recovered with reasonable accuracy, with the trial profile being the most affected. Shown in the examples (Fig 3, bottom), the effect of noise on the trial profile can be observed as a shrinking of the ratios between loadings of trials with a different number of simulated network sequences and an increase in the trial profiles ‘baseline’; the loadings of those trials which had 0 network sequences. The latter is important in practice, because under the assumption that a network is not active in all trials, the lowest trial loadings w.r.t. to the higher trial loadings can be used as an indication of the reliability of network parameters. Secondly, we observe that, except from the largest jitter case ( $\pm 2\text{ms}$ ), network spike jitter has a similar effect on recovery of network parameters as spiking noise, as evidenced by the similarity between the e.g. 10Hz/0ms and the 5Hz/ $\pm 0.25\text{ms}$  cases, and the 20Hz/0ms and the 5Hz/ $\pm 0.5\text{ms}$  cases. Regarding network specific recovery, though there was some variation in recovery, the differences were minimal and did not highlight a sensitivity to a particular aspect of the simulated networks.

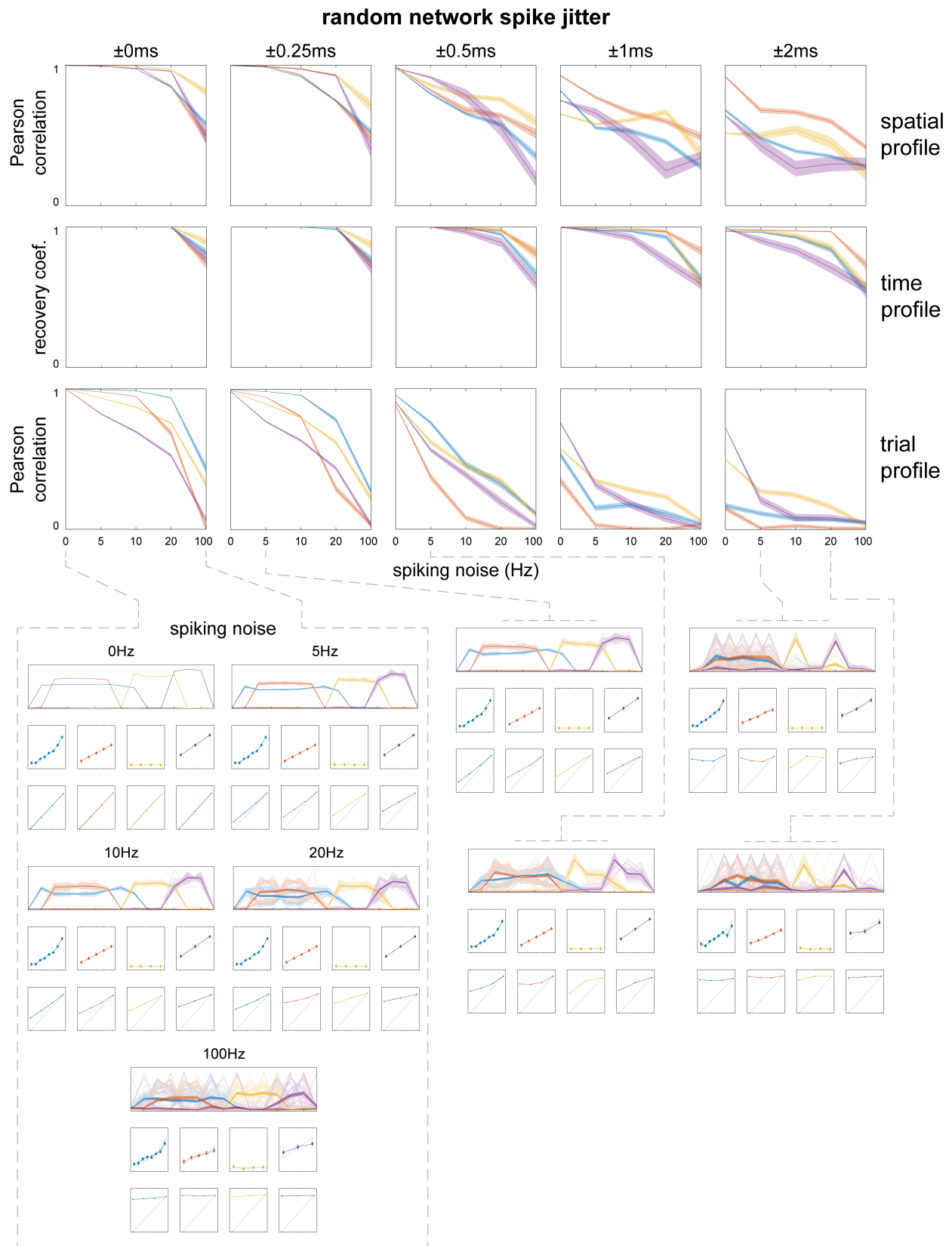


**Figure 3. Recovery of simulated spike timing networks with spiking jitter and spiking noise.** Networks were simulated 50 times at 5 levels of spiking jitter and 5 levels of spiking noise. Recovery of the spatial and trial profiles are shown as Pearson correlations

between the extracted and simulated networks (ranged from -1 to 1, visualized from 0 to 1). The recovery of the time profile is shown by a recovery coefficient ranging from 0 to 1 (perfect recovery). Networks are colored as in Figure 2. Bottom panels visualize extracted networks as in Figure 2 at several example jitter and noise levels. Spatial profiles are shown as means over simulations (shading = STD), with that of individual simulations as thin transparent lines. Time profiles are displayed as average over simulations (error bar = STD; aligned using average difference between simulated and recovered networks). Trial profiles show means over trial weights per # of simulated sequence repeats, averaged over simulations (error bar = STD). The simulated trial profiles and time profiles are indicated in gray for reference. Note that, (1) when spiking noise and jitter increases, the trial profiles ‘baseline’ (weights of non-contributing trials that should be 0) gradually increases, (2) spiking noise has a stronger effect on the trial profiles of networks with fewer neurons, and, (3) the time profiles are more robust to noise than the spatial profiles and trial profiles, with accurate recovery even when spike jitter is a multiple of the between-neuron time delays. Also note in the examples that as noise increases, matching of simulated networks to extracted networks becomes troublesome, leading to differences between network-specific recovery becoming less meaningful. See Materials and Methods section 5 and 6.

### **3. Recovery of simulated spike timing networks with sparse spiking when surrounded by spiking noise**

It has been shown that even when neurons fire selectively to a stimulus, they don’t do so every instance of the stimulus. That is, neurons tend to fire sparsely (Barth and Poulet, 2012). To investigate how sparseness in spike timing networks, i.e. not all member neurons joining in each spike sequence, affects characterization of the full spike sequences, we simulated networks where each spike of a sequence had a chance to be deleted. Similar to the above, we did so 50 times for each level of spike deletion probability, and of spiking noise. The results are shown in Figure 4. We observe that, (1) as the chance of spike deletion increases, recovery accuracy decreases, (2) as with spiking jitter/noise, the trial profile is more affected by noise than the spatial profile, (3) as with spiking jitter/noise, the effects of spike deletion on recovery are similar to those of spiking noise, and, (4) the full spike sequences in the time profile are accurately extracted under reasonable noise (20Hz) with 40% probability of spike deletion, even though the majority of individual spike sequences were incomplete. As in the above, the minor differences in recovery of specific networks did not indicate a subset of networks to be specifically impacted by sparse spiking.

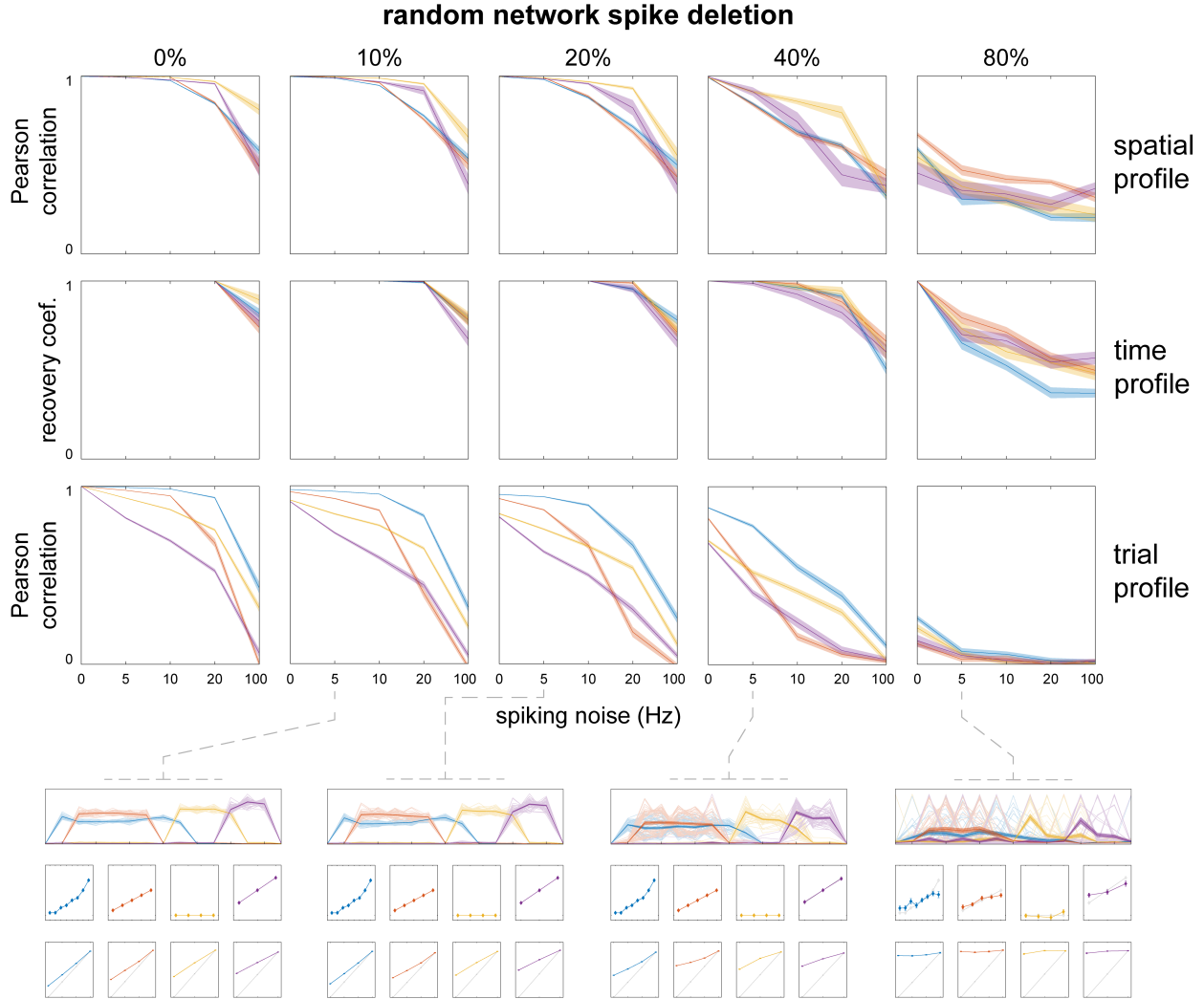


**Figure 4. Recovery of simulated spike timing networks with sparse network spiking and spiking noise.** Networks were simulated 50 times at 5 probability levels of spike deletion, and 5 levels of spiking noise. Probability is the chance for each individual (non-noise) spike to be deleted. Recovery and examples are displayed identically to Figure 3. Note that, (1) the effect of spike deletion affects the spatial profiles, time profiles, and trial profiles similarly to that of spike jitter and spiking noise, and, (2) even when the spiking sequences of each networks are very unreliable (80% chance of each spike's absence) the networks can still be identified in the examples at 5Hz spiking noise. See Materials and Methods section 5 and 6.

#### 4. Cross spectra normalization diminishes effects of differential firing rates of units and trials

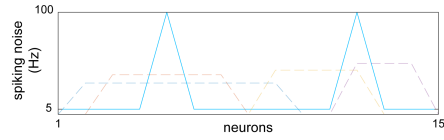
The spike timing networks simulated above were extracted under noise related firing rates that were identical over neurons and over trials. This was chosen to show the overall effect of spiking noise, and is atypical for real recordings. Here, we show the effect of differential noise related firing rates over neurons and trials on the recovery of simulated networks.

We first show the recovery of simulated networks when the firing rate differs over neurons (Fig 5). We simulated networks 50 times, with neuron 5 (a member in network 1 and 2) and neuron 12 (member in network 3 and 4) having 100Hz spiking noise, the other neurons 5Hz (Fig 5A). Network spiking jitter was  $\pm 0.25\text{ms}$ . The recovery of the networks (Fig 5B; compare to Fig 2) is distorted: (1) the spatial profiles of the networks for neurons 5 and 12 are strongly increased/decreased, (2) the noise of neuron 5 leads to a strong loading for network 3, of which it is not a member, (3) network 4 is dominated by neuron 12, (4), the trial profiles show decreased recovery (compared to Fig 2), and (5) although the time profile of networks 1, 2, and 4 are not (noticeably) distorted, network 3's is. Overall,

the differential firing rate can be said to pull the estimated network parameters towards those neurons with more spiking. This effect however, can be substantially reduced by normalizing cross spectra prior to network extraction. Here, we show the effect of normalizing cross spectra such their power is equal to their Nth root (see Materials and Methods section 4), reducing differences in firing rates. We show its effects progressively by using  $N = 2, 4, 8, 16, 32$  (Fig 5C), and ending with  $N = 64$  (Fig 5D). We observe that (1) the recovery of the spatial profiles is improved, with network 1 showing the most remaining distortion at neuron 5, (2) the trial profiles are similar to the case with 5Hz spiking noise for all neurons (see Fig 2), and, (3) the recovery of the time profile of network 3 is improved such that the distortion is minimal.

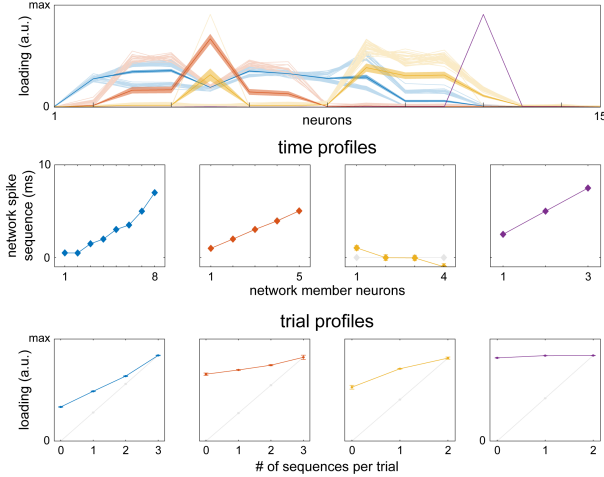
To investigate the effect of differential spiking rate over trials we simulated networks with 5Hz spiking noise, except for trials 21 to 60, which had 10Hz spiking noise (Fig 6A). Network spiking jitter was set at  $\pm 0.25\text{ms}$  spiking jitter, and networks were simulated 50 times. The trials with additional spiking noise were chosen such that they both involved 100% of trials of sequence repeats (1x and 2x for network 1, 1x for network 2, 1x for network 4) and a partial set of sequence repeats (50% of 1x and 2x for network 3, 50% of 0x for network 2). The recovery without normalization is shown in Figure 6B. We observe that (1) the recovery of the spatial profiles and time profiles are similar to the case of 5Hz noise and  $\pm 0.25\text{ms}$  spiking jitter (see Fig 2) and, as such, are minimally affected by the differential noise over trials, and, (2) the trial profiles' loadings for the trials affected by the noise are distorted such that the ratios of loadings no longer reflect the correct order of the number of sequence repeats (e.g. 1x trials are higher than 2x trials for network 4). As was the case for differential noise over neurons, normalization of the affected dimension can improve recovery. Here, we normalized the cross spectra such that the power of every trial is equal to the power summed over trials (see Materials and Methods section 4). Crucially, this does not affect the ratio of the off-diagonal elements to the diagonal (power). As such, trials that have many spike sequences (strong off-diagonal elements compared to power) are still distinguishable from trials with few spike sequences (weak off-diagonal elements compared to power). Note, as well, that this trial-wise normalization is unrelated to the neuron-wise normalization applied above, and they can be applied jointly. We show the result of the trial-wise normalization in Figure 6C. We observe that, (1) the trial profiles' recovery is improved such that the order of their loadings again reflects the order of the number of sequence repeats, and, (2) though improved, the trial profiles' recovery is poorer than those at equal noise levels for all trials (see Fig 2). We additionally observe that the normalization also affected the trial profile loadings of trials that did not have increased noise. This is most noticeable in the loadings for those trials of network 4 that had 0 and 2 sequence repeats (trials 1 to 20 and 61 to 100): the ratio of the loading of 0 repeats to that of 2 repeats is much higher without normalization (Fig 6B), than with normalization (Fig 6C). As trials with 0 repeats should ideally have a loading of 0, the higher this ratio the better.

### A neuron-specific spiking noise



### B no normalization

spatial profiles



### C normalization: power =

$$\text{power}^{1/2}$$

$$\text{power}^{1/4}$$



### D normalization: power = power^{1/64}

spatial profiles

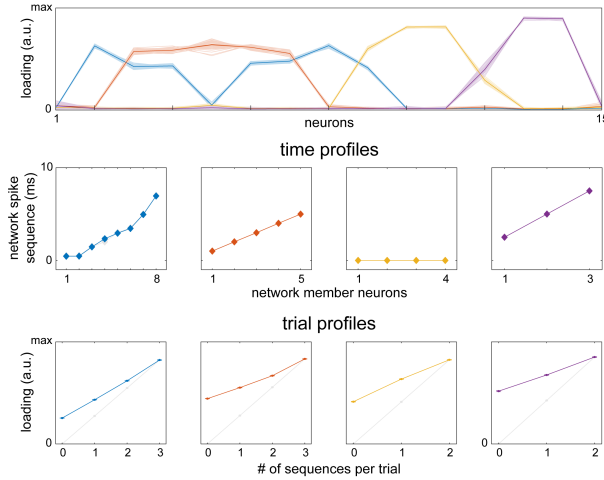


**Figure 5. Cross spectra normalization diminishes effects of differential neuron firing rates.** In realistic neuron recordings, the firing rate of neurons typically differ. To show the effect of differential firing rates on network recovery, we simulated spike timing networks (spiking jitter =  $\pm 0.25$ ms; spike deletion = 10%) 50 times with two neurons having 100Hz spiking noise, the other neurons 5Hz. To improve performance, the cross spectra can be normalized. Specifically, when normalized such that the diagonal of the cross spectra becomes its  $n$ th root, network recovery is improved. **A**, spiking noise as a function of neurons, with the simulated spatial profiles in the. **B**, network recovery without normalization. Though the networks are recognizable, recovery is clearly affected. Networks are displayed identically to examples in Figure 3. **C**, the effect of square, 4<sup>th</sup>, 8<sup>th</sup>, 16<sup>th</sup>, 32<sup>nd</sup> root power normalization on recovered networks, culminating in: **D**, recovered networks after 64<sup>th</sup>-root power normalization. See Materials and Methods section 4 and 5.

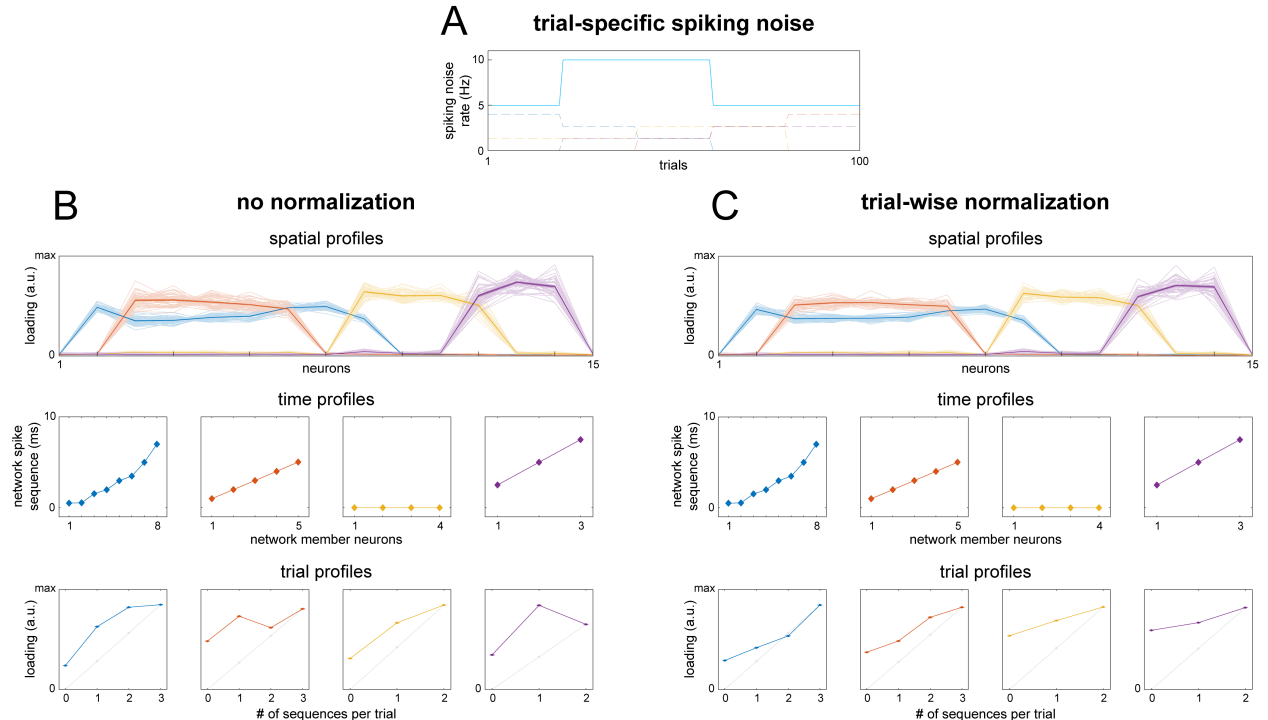


**Figure 6. Trial-wise cross spectra normalization diminishes effects of differential trial firing rates.** In realistic recordings, the firing rate of neurons typically differs over trials. To show its effect on network recovery, we simulated spike timing networks (spiking jitter =  $\pm 0.25$ ms; spike deletion = 10%) 50 times with 40 trials having 10Hz spiking noise (for all neurons), the other trials 5Hz. To improve performance, the cross spectra can be normalized in a similar way as for differential neuron firing rates. Specifically, the cross spectra of each trial can be normalized such that its diagonal, is equal to that of the cross spectra summed over trials. **A**, spiking noise as a function of trials, with the simulated trial profiles in the background. **B**, recovered networks with trial-wise normalization. Networks are displayed identically to examples in Figure 3. The trial profiles of the recovered networks are strongly affected. **C**, like B but for networks recovered after trial-wise normalization. While the trial profiles still deviate from the simulated networks, the ratios of their weights w.r.t. the # of simulated sequence repeats is partially restored. See Materials and Methods section 4 and 5.

## 5. Spike timing networks extracted from real recordings reflect between-neuron spike timing relationships

To provide a proof-of-principle we extracted spike timing networks extracted from spike recordings from medial prefrontal cortex and hippocampus of a rat performing an odor-based delayed matching-to-sample task (Fig 7; see Materials and Methods section 7). After odor presentation, the rat had to run through the left or right arm of a figure-eight T-maze to obtain its reward. Networks were extracted similarly to the simulations above, using a neuron-wise 32<sup>nd</sup> root power normalization, and a split-half reliability approach to determine the number of networks (see Materials and Methods section 2). This resulted in 4 extracted networks.

We show spatial profiles, time profiles, and trial profiles for each extracted spike timing network in Figure 7. To provide a ground-truth estimate of whether the between-neuron spike times from the networks reflect real spike timing relationships in the recordings, we also show for each network continuous cross-correlograms (see Materials and Methods section 7) of the neurons mostly strongly contributing to each network. Importantly, in each of these cross-correlograms we indicate when the cross-correlation should be highest, based on the time profile of the networks.

For network 1, neuron pairs 1-2, 1-3, and 2-3 had peaks in their cross-correlograms that matched the time profile's spike timing relationships within 0.03ms, 0.03ms, and 0.06ms respectively. Neuron 4 does not appear to have consistent spike timing relationship with the first three, which is unsurprising given that its weight in the spatial profile is much weaker (suggesting its weight reflects, at least mostly, noise). Although there appears to be a difference in network activity between left and right trials, this is likely caused by firing rate differences between conditions, as trial profiles calculated on trial-wise normalized cross spectra did not differ between conditions, nor did cross-correlations that controlled for firing rates (Pasquale et al., 2008). For network 2, neuron pairs 1-2, 1-3, and 1-4 had cross-correlogram peaks that matched the time profile within 0.09ms, 0.07ms, and 0.19ms respectively. Neuron pair 2-3 and pair 3-4 did not have single cross-correlogram peak (though their center peaks matched within 0.17ms and 0.12ms resp.), and neuron pair 2-4 appears inhibitory. These observations could indicate that the spike sequence did not involve all 4 neurons in a subset of trials. It is useful to reiterate here, that the extracted spike sequence should be considered only at the level of the full recording (i.e. cross spectra of all trials). That is, the extracted spike sequence should be considered as a description of the N-way relationship between N neurons, i.e. the largest possible spike sequence for the network, and serve as a starting point for targeted analyses. Network 3 show a similar pattern as network 1 and 2 according the cross-correlograms, with the peaks of neuron pairs 1-2, 1-3, 1-4, and 2-3, matching the time profile within 0.10ms, 0.09ms, 0.05ms, and 0.19ms resp. Network 4 likely reflects consistent spike timing only between the strongest two neurons (matching within 0.08ms), as the spatial profile has few neurons with strong loadings.

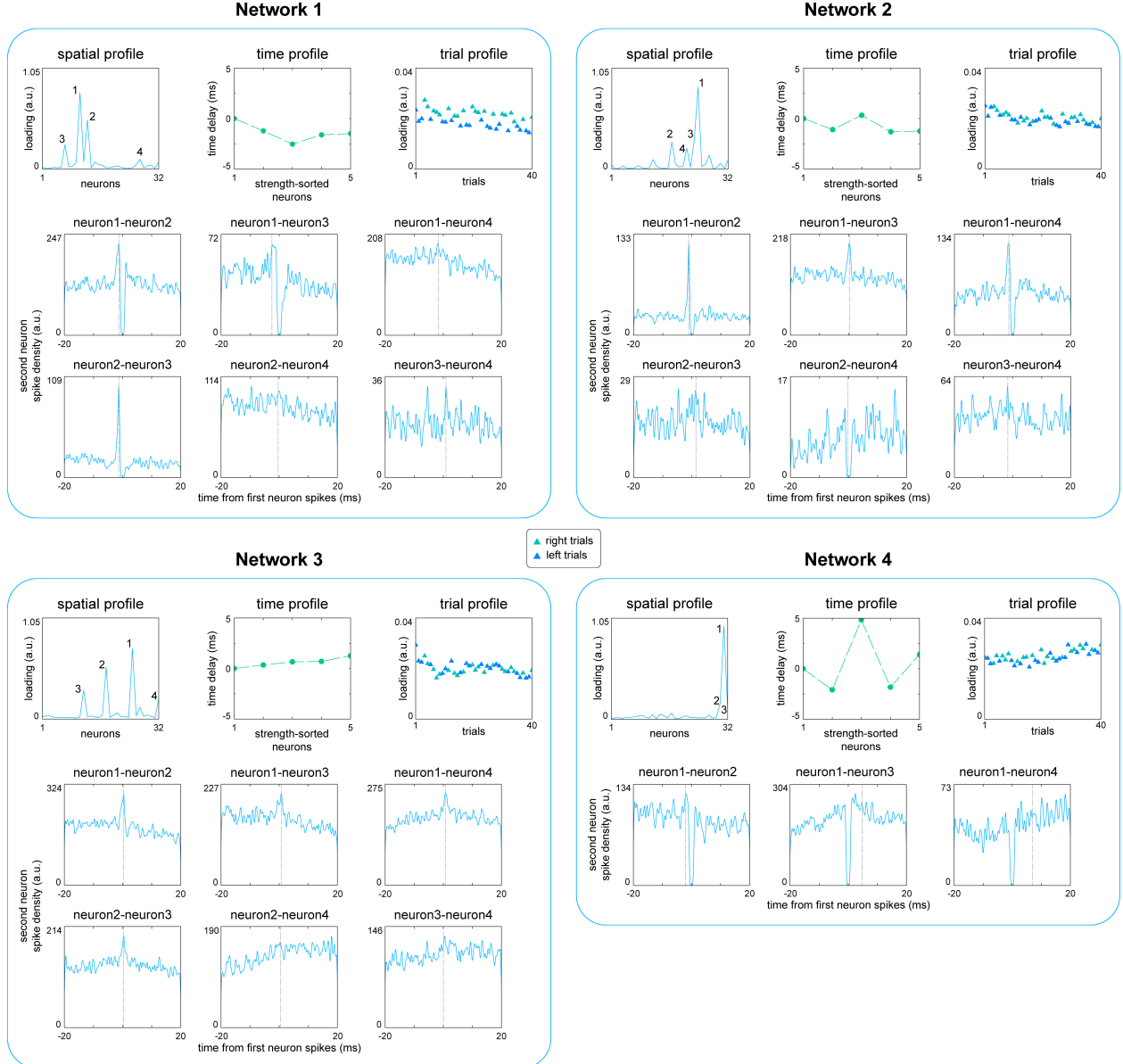


**Figure 7. Example spike timing networks extracted from rat medial prefrontal cortex and hippocampus.** We extracted 4 spike timing networks from recordings in which a rat either had to take the left or right arm of a figure-eight T-maze. The number of networks to extract was estimated using a split-half approach. The first row of each network shows the spatial profile, the time profile, and the trial profile. The time profile only shows the strongest 5 neurons of the trial profile (as given by the spatial profile). Several of the strongest neurons are highlighted in each spatial amplitude map. To show that the networks reflect spike timing consistencies in the data, we also show cross-correlograms in the second and third row. The cross-correlograms of each pair of the highlighted neurons are shown as spike densities, the y-axis limit roughly reflects spike counts. The dashed gray line is the time delay between the neurons as given by the time profile of the network. We observe the following. For network 1, neuron pairs 1-2, 1-3, and 2-3 the extracted time delays are close to the cross-correlogram. Though the 4<sup>th</sup> neuron has a higher weight than the non-highlighted neurons in the spatial profile, the cross-correlograms are not as strongly peaked as for the other pairs. For network 2, the extracted time delays of pairs 1-2, 1-3, 1-4 are closest to their cross-correlograms. Though for network 3 the cross-correlograms show weaker spike timing consistency (higher baseline spike density), the extracted time delays of pair 1-2, 1-3, 1-4, and 2-3 are close to their peaks. Network 4 involves few strong neurons, as indicated by the spatial profile; only the neuron pair 1-2 is close to its peak. See Materials and Methods section 7.

## References

- Barth AL, Poulet JFA (2012) Experimental evidence for sparse firing in the neocortex. *Trends Neurosci* 35:345–355.
- Fujisawa S, Amarasingham A, Harrison MT, Buzsaki G (2008) Behavior-dependent short-term assembly dynamics in the medial prefrontal cortex. *Nat Neurosci* 11:823–833 Available at: <http://dx.doi.org/10.1038/nn.2134>.
- Fujisawa S, Amarasingham A, Harrison MT, Buzsáki G (2014) Simultaneous electrophysiological recordings of ensembles of isolated neurons in rat medial prefrontal cortex and intermediate CA1 area of the hippocampus during a working memory task.
- Pasquale V, Massobrio P, Bologna LL, Chiappalone M, Martinoia S (2008) Self-organization and neuronal avalanches in networks of dissociated cortical neurons. *Neuroscience* 153:1354–1369.
- Rossant C, Kadir SN, Goodman DFM, Schulman J, Hunter MLD, Saleem AB, Grosmark A, Belluscio M, Denfield GH, Ecker AS, Tolias AS, Solomon S, Buzsaki G, Carandini M, Harris KD (2016) Spike sorting for large, dense electrode arrays. *Nat Neurosci* 19:634–641 Available at: <http://dx.doi.org/10.1038/nn.4268>.
- van der Meij R, Jacobs J, Maris E (2015) Uncovering phase-coupled oscillatory networks in electrophysiological data. *Hum Brain Mapp* 36:2655–2680.
- van der Meij R, van Ede F, Maris E (2016) Rhythmic Components in Extracranial Brain Signals Reveal Multifaceted Task Modulation of Overlapping Neuronal Activity. *PLoS One* 11:e0154881.